SUPPLEMENTARY DATA

The human telomeric nucleosome displays distinct structural and dynamic properties

Aghil Soman, Chong Wai Liew, Hsiang Ling Teo, Nikolay Berezhnoy, Vincent Olieric, Nikolay Korolev, Daniela Rhodes and Lars Nordenskiöld[1]*

Supplementary Figure S1

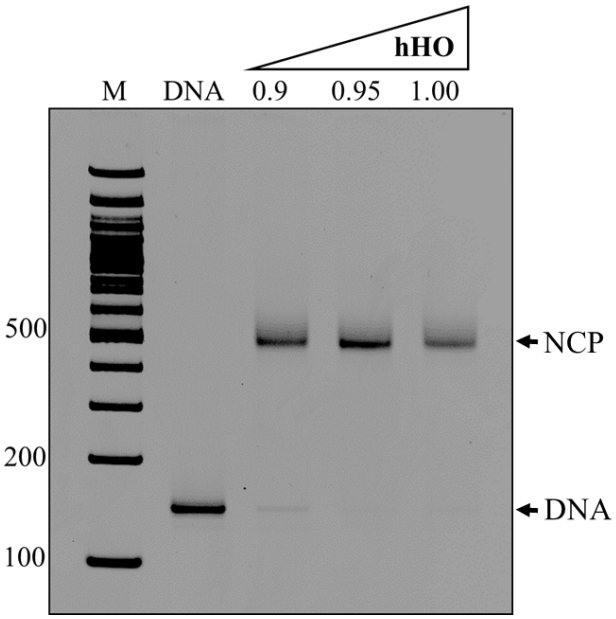

Supplementary Figure S1. Reconstitution of Telo-NCP. Lane M is DNA marker, lane DNA is reference 145 bp telomeric DNA and lanes 0.9, 0.95 and 1.00 show products of the Telo-NCP reconstitution with the respective human HO:DNA ratios.

Supplementary Table S1. Anomalous data statistics for the telomeric NCP (dataset 1, two orientations).

	Manganese	Phosphorus	Cobalt
Beamline (Synchrotron Station)	X06DA (SLS)	X06DA and X06SA (SLS)	X06DA (SLS)
Number of crystals used	1	2	1
Total oscillation (χ /φ orientations)	15 x 360º, 0.1s, 0.2º • φ = 0º / χ = 0º, 15º, 25, 30º and 35º • φ = 90º / χ = 0º, 15º, 25, 30º and 35º • φ = 180º / χ = 0º, 15º, 25, 30º and 35º	**Crystal 1:** 35 x 360º, 0.1s, 0.2º • φ = 0º / χ = 0º, 10º, 15º, 20º, 25º, 30º and 35º • φ = 45º / χ = 0º, 10º, 15º, 20º, 25º, 30º and 35º • φ = 90º / χ = 0º, 10º, 15º, 20º, 25º, 30º and 35º • φ = 135º / χ = 0º, 10º, 15º, 20º, 25º, 30º and 35º • φ = 180º / χ = 0º, 10º, 15º, 20º, 25º, 30º and 35º **Crystal 2**: 24 x 360º, 0.1s, 0.1º • φ = 30º / χ = 10º, 15º, 20º, 25º, 30º and 35º • φ = 60º / χ = 10º, 15º, 20º, 25º, 30º and 35º • φ = 120º / χ = 10º, 15º, 20º, 25º, 30º and 35º • φ = 150º / χ = 10º, 15º, 20º, 25º, 30º and 35º	7 x 360º, 0.1s, 0.2º • φ = 0º / χ = 0º, 15º and 25 º • φ = 45º / χ = 0º, 15º, 25º and 30º
Resolution (Å)	50.0 – 3.2	50.0 – 2.9	50.0 – 3.42
Space group	$P2_12_12_1$	$P2_12_12_1$	$P2_12_12_1$
Cell dimensions *a*, *b*, *c* (Å) α, β, γ (º)	 106.21, 109.16, 176.32 90.0, 90.0, 90.0	 106.15, 109.15, 175.95 90.0, 90.0, 90.0	 106.38, 109.23, 176.70 90.0, 90.0, 90.0
No. of reflections	9,906,543 (655,417)	31,036,376 (2,103,663)	2,805,628 (159,227)
No. of unique reflections	136,513 (7,738)	134,436 (8,313)	82,587 (5,620)
Redundancy	15.1	14.7	17.6
Completeness (%)	99.6 (99.5)	98.3 (98.5)	99.1 (99.8)
$\langle I/\sigma(I) \rangle$ [a]	8.29 (1.05)	29.91 (1.03)	11.7 (1.47)
$CC_{1/2}$ (%)	100 (85.2)	100 (92.1)	100 (85.2)
Anomalous completeness	99.9	99.7	100.0
Anomalous multiplicity	18.1	17.9	12.3
CC_{ano}	0.13	0.19	0.12
Mosaicity (º)	0.23	0.21	0.14

Supplementary Figure S2

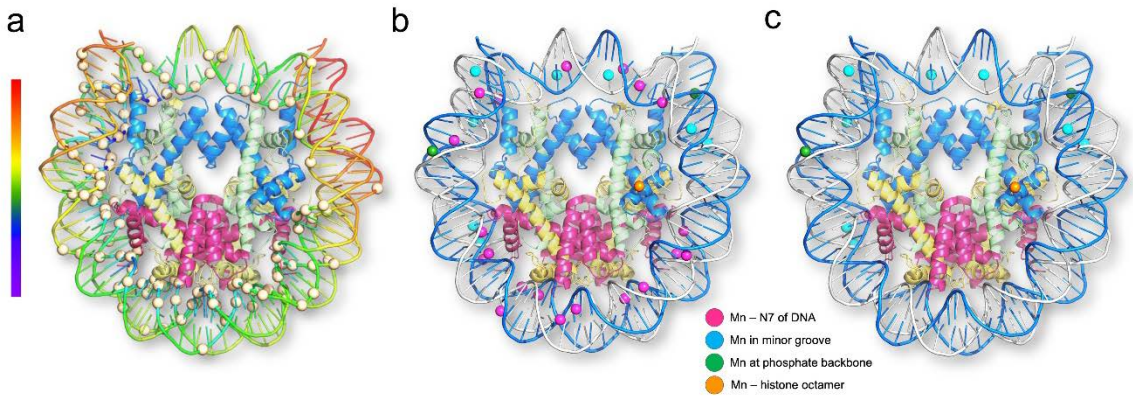

Supplementary Figure S2. A solution of the structure of the two-orientation telomeric NCP. The initial structure was obtained by molecular replacement and by rebuilding the bases from DNA phosphate location as inferred from the phosphorous anomalous map (**a**) Location of phosphorous atoms determined from the phosphorous anomalous map. 114 phosphorous atoms (light yellow spheres) that can be confidently located were used to build the DNA structure. The DNA is plotted by temperature factors. Refinement of the rebuilt structure resulted in diffused densities for the bases of the DNA indicating averaging over two orientations. To verify this, we collected manganese and cobalt single-wavelength anomalous datasets (Supplementary Table S1). Mn^{2+} and Co^{2+} ions coordinate with N7 and O6 of guanine in 'GG' or 'GC' steps of the major groove and in the telomeric nucleosomes will only bind to one of the DNA strands. **(b)** The overall distribution of Mn^{2+} ions on the telomeric NCP. Mn^{2+} coordination with the N7 of guanine is shown as pink spheres. (**c**) Distribution of Mn^{2+} ions that do not coordinate with the N7 of guanine. Mn^{2+} ions located near the phosphate backbone, histone octamer and minor groove are displayed as green, orange and blue spheres respectively.

Supplementary Figure S3

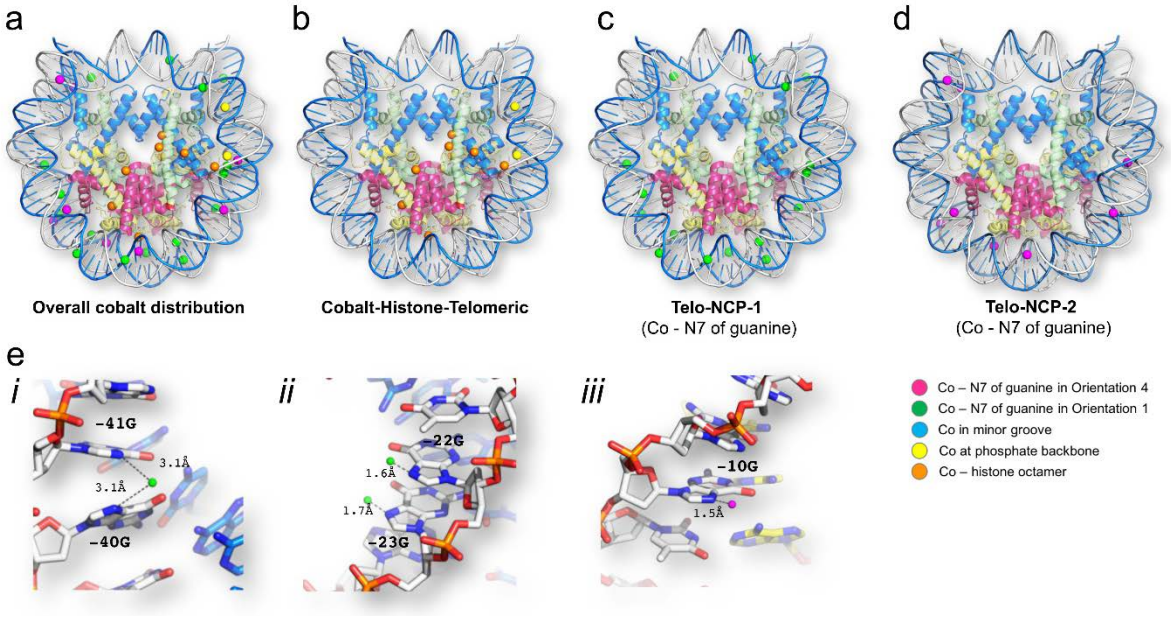

Supplementary Figure S3. Locations of the Co^{2+} ions in the Telo-NCP. **(a)** The overall distribution of Co^{2+}in the Telo-NCP. Co^{2+} coordination to the guanines N7 in the major groove of the Telo-NCP-1 is shown as magenta spheres and those interacting with the guanine N7 in the Telo-NCP-2 are depicted as green spheres. Co^{2+} coordination to the phosphate backbone, histone octamer and minor groove is shown as yellow, orange and blue spheres respectively. **(b)** Co^{2+}coordination to the histone octamer and phosphate backbone. **(c)** Co^{2+} coordination to the guanine N7 in the Telo-NCP-1. **(d)** Co^{2+} interaction with guanine bases in the Telo-NCP-2. **(e)** Two modes of Mn^{2+} coordination to the guanine N7 are also observed for Co^{2+}. Examples of Co^{2+} coordination with the single guanine N7 and with the two adjacent guanine N7 atoms are shown.

Supplementary Table S2. Refinement statistics of the dataset-2 with a single orientation of the NCPs in the crystal lattice. Refinements were carried out to investigate the preference for single orientation with full occupancy (without anisotropy correction) and half occupancy (with anisotropy correction). Without anisotropy correction, we did not notice significant preference, but with half occupancy and anisotropy correction, there was a clear preference for orientation 1. Omit maps were also created with deletion of guanine bases, followed by refinement with filling in with the four DNA bases. The refinement statistics and the maps from one such deletion of base −28I is shown below and in Supplementary Figure S4 below.

Dataset	Orientation 1 (R_{work}/R_{free})	Orientation 2 (R_{work}/R_{free})
Datatset-2 (without anisotropy correction)	26.7/29.2	26.7/29.5
Datatset-2 with half occupancy (2.2 Å)	29.4/34.0	32.2/36.2
Refinement statistics after fill in at position −28I (2.2 Å)		
DNA base used for fill in	R_{work}/R_{free}	
Adenine	26.6/33.3	
Thymine	26.6/33.3	
Cytosine	26.6/33.3	
Guanine	26.6/33.2	

Supplementary Figure S4

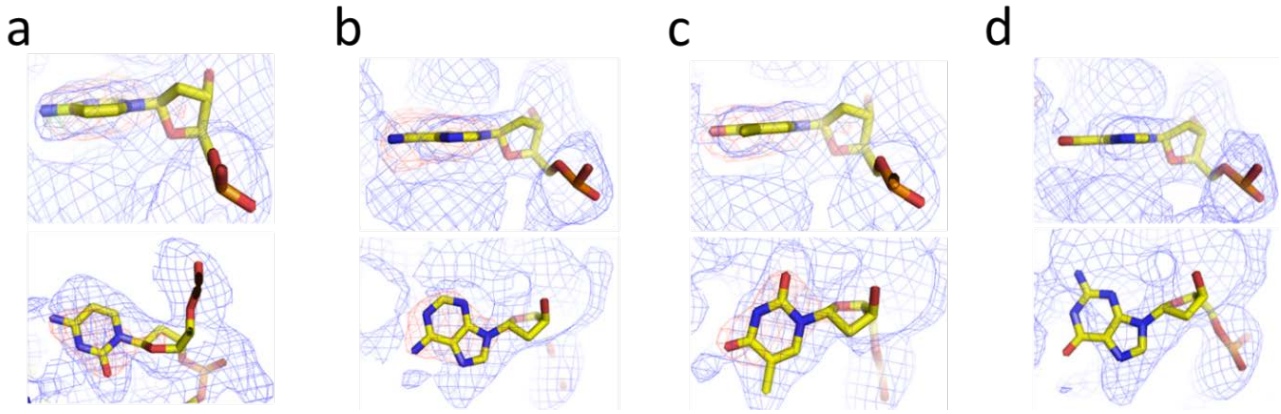

Supplementary Figure S4. Refinement with omit maps indicating the presence of the NCP in single orientation in the dataset 2. Omit maps were generated by deletion of guanine bases (an example for the −28I position is shown). The four DNA bases cytosine (a) adenine (b), thymine (c) and guanine (d) were used to 'fill in' for the missing nucleotide and refined. The side view and top view of the nucleotide at position −28I after the refinements superimposed with the blue (named 2Fo−Fc) (1σ) and red (Fo−Fc) (3σ) density map are shown. The maps from the refinements with adenine, thymine and cytosine display intensity in the Fo−Fc maps in (a), (b) and (c), indicative of an incorrect fit with the electron density at −28I. Refining the structure with guanine gave a correct fit, confirmed by the absence of the red density in the Fo−Fc map in (d). In an NCP crystal with two orientation, the position −28I in the second orientation will be occupied by cytosine and refinement with cytosine would not have given a Fo−Fc map density. Multiple other locations occupied by guanines were also investigated and gave similar results confirming that presence of a single orientation in dataset 2.

Supplementary Figure S5

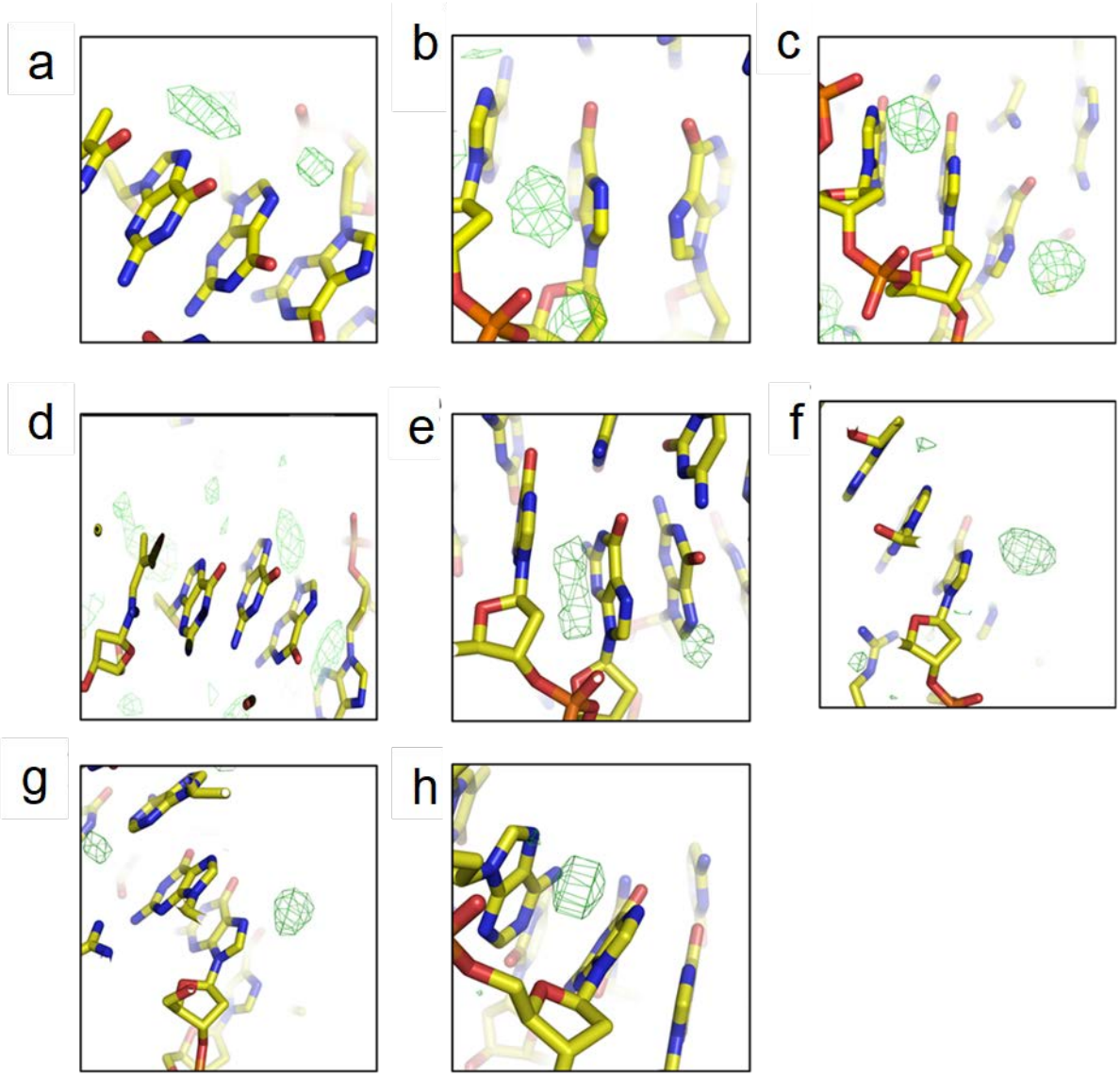

Supplementary Figure S5. Putative Mn^{2+} electron densities (shown in green) in the Telo-NCP crystal of the dataset-2 with a suggested single NCP orientation. The putative Mn^{2+} densities are visible in the Fo−Fc map at the expected coordination distance near the guanine N7. These signals at coordination distance from N7 of guanine were investigated for both orientations. The densities are stronger (higher σ) and more numerous in the dataset-2 comparing to the similar signals observed in the electron density map of the dataset-1 where two orientation of the Telo-NCP is observed (see Fig. S6). This is a confirmation that most of the NCPs are in a single orientation in the dataset 2. The locations of putative signals in the Telo-NCP orientation 1, dataset 2 are presented at the positions **(a)** −64I, −65I and −66I. **(b)** −13I, −12I, −11I. **(c)** −5I, −6I, −7I. **(d)** 5I, 6I, 7I. **(e)** 24I, 25I 26I. **(f)** 35I, 36I, 37I. **(g)** 48I, 49I 50I. **(h)** 60I, 61I and 62I. The image is rendered with coot (Fo−Fc map −3σ)

Supplementary Figure S6

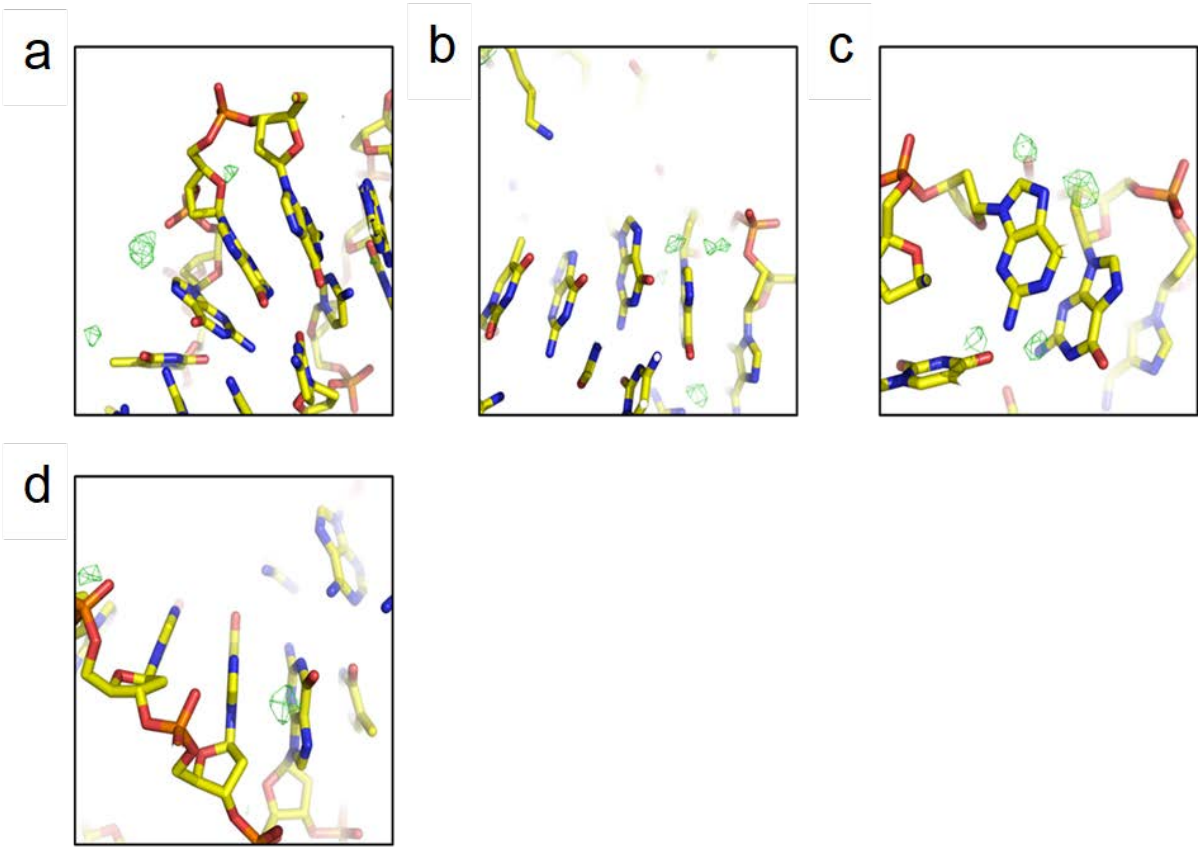

Supplementary Figure S6. Putative Mn^{2+} electron densities for the Telo-NCP in orientation 2 of the dataset-2. The signals at coordination distance from N7 of guanine of the orientation 2 were fewer in number and weaker. The locations of putative signals (green blobs) in orientation 2 are presented **(a)** −28J. **(b)** 7J. **(c)** 13J. **(d)** 38J. (Fo−Fc map −3σ).

Supplementary Figure S7

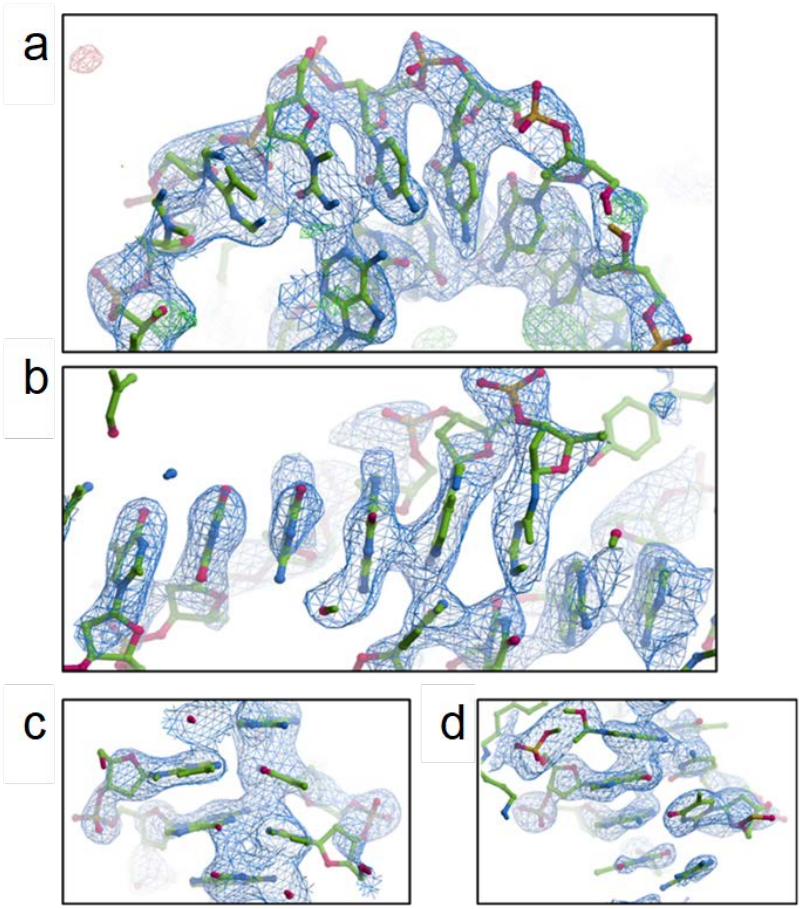

Supplementary Figure S7. Snapshots from the electron density map of 2.2 Å Telo-NCP structure. The DNA from dataset-2 shows well-defined electron density with base separation. Map rendered with COOT (1) at a contour level of 1.49σ. (**a**) SHL 2. (**b**) SHL 6.5. (**c**) Dyad. (**d**) SHL −7. Note: The map shown is from refinements carried out with REFMAC.

Supplementary Figure S8

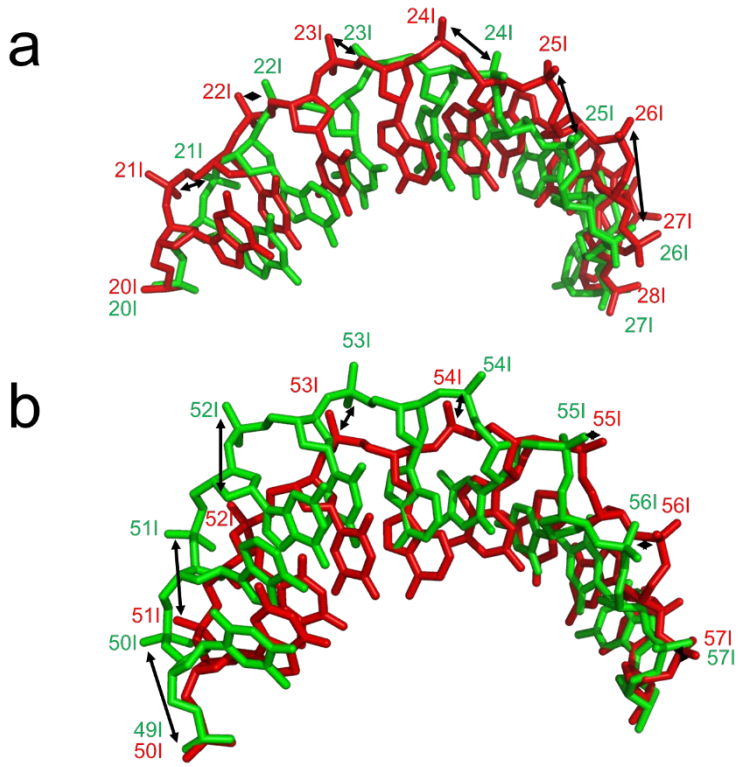

Supplementary Figure S8. Comparison of DNA path in the Telo-NCP crystal with the palindromic 145 bp alpha satellite sequence (α-sat-NCP, PDB code 2NZD (1)). Telo-NCP is shown in red, the α-sat-NCP structure is in green. There are two regions of deviation, the deviations in the positive half of NCP is shown (SHL 0-7). **(a)** The stretching of DNA in the α-sat-NCP from 20I to 27I (SHL 2 to SHL 2.5) is missing in Telo-NCP. The double-headed black arrow indicates the deviation between corresponding phosphates. The DNA phosphates of the two NCPs are in phase until 20I. The stretching across bases 20I to 28I is characterized by increasing difference in positions of the corresponding bases. By the base pair 28I, the phosphates are out of phase by one bp with respect to the corresponding atoms of the α-Sat-NCP. The DNA remains out of phase by one base pair from 28I to bp 50I (SHL 2.5 to SHL 5). **(b)** The stretch across 50I to 57I (SHL to SHL 5.5) by one bp on the Telo-NCP brings the phosphate back in phase with the phosphates of the alpha satellite NCP.

Supplementary Table S3. Base steps at pressure points where the minor groove faces inward for the Telo-NCP 2.2 Å-resolution structure as well as for the Telo-NCP-1 2.5 Å-resolution orientation 1 structure (dataset 2 with two orientations of the NCP in the crystal lattice). Comparison with α-sat NCP (1) NCP-601 (2) and NCP-601L (3). All NCPs consist of 145 bp DNA.

SHL	Telo-NCP, dataset 2, one orientation	Telo-NCP, dataset 1, two orientations	α-sat NCP (2NZD)	601 NCP (3LZ0)	601L NCP (3UT9)
−5.5	TA	TA	AG	CG	CG
−4.5	GG	GG	AA	TC	TC
−3.5	GG	GG	TG	TA	TA
−2.5	TA	TA	TC	TA	TA
−1.5	TT	TT	GG	TA	TA
−0.5	GG	GG	AG	TA	TA
0.5	AG	AG	CT	CC	TA
1.5	TT	TT	CC	TA	TA
2.5	GG	GG	GA	GG	TA
3.5	AG	AG	CA	CC	TA
4.5	TA	TA	TT	AG	GA
5.5	GT	GT	CT	TC	CG

Supplementary Figure S9

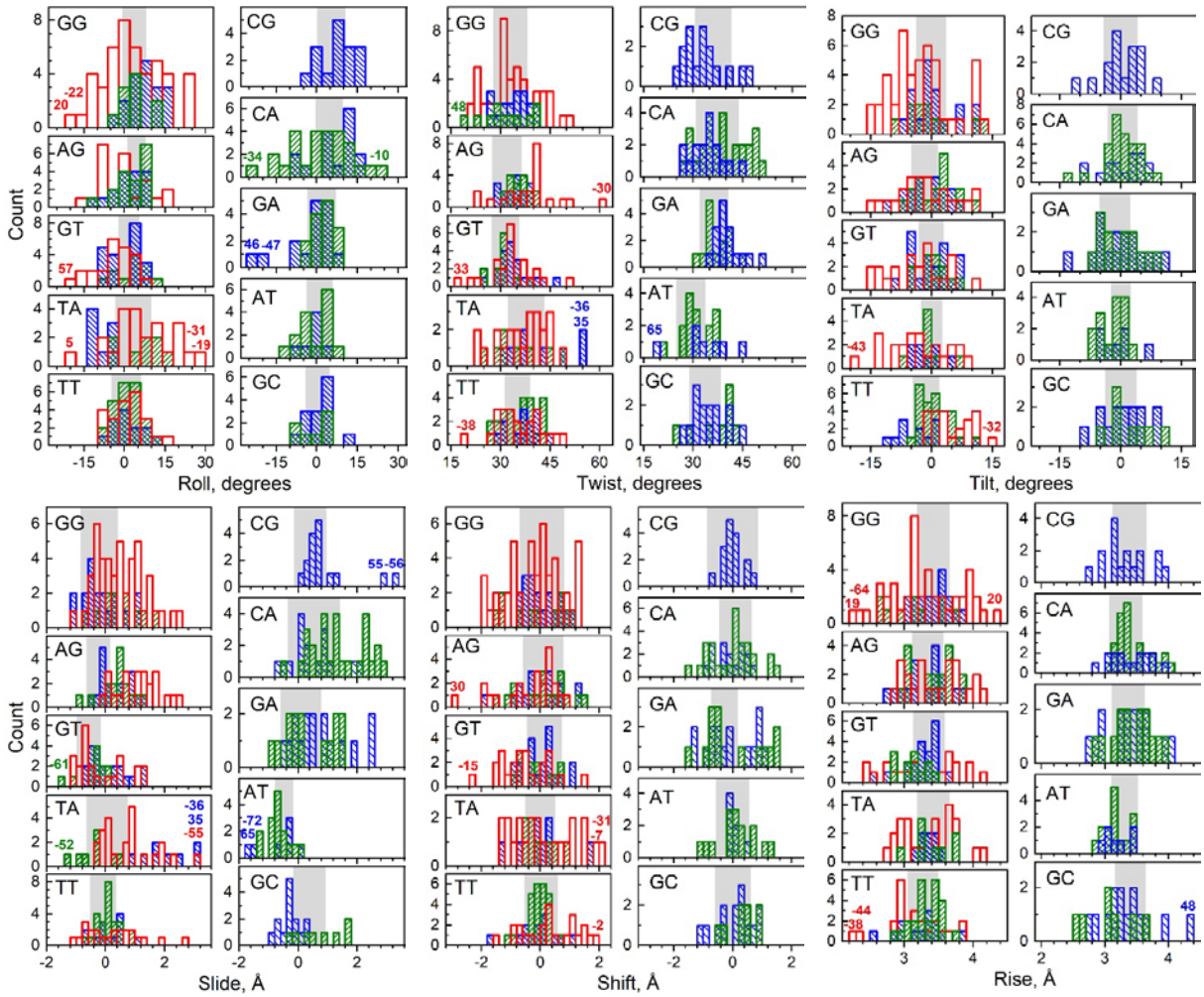

Supplementary Figure S9. Population distribution of base-pair step parameters in the Telo-NCP in comparison with the same steps present in the NCP-601L and α-satellite NCP. Base steps from Telo-NCP, NCP-601L and α-satellite NCP are shown respectively as red, blue and green columns. In each panel, the shaded area covers the range of values (mean ± s.d.) observed in DNA crystals according to the analysis by Olson et al (4). Coloured numbers mark base-pair step positions of extreme deviation of the respective parameters. It may be noted that the Telo-NCP GT base step 15 exhibits an extreme tilt value of 36 degrees and is outside the display range and not shown in the corresponding figure. Some of the more pronounced deformation cases observed in the Telo-NCP are illustrated in Supplementary Figure S10 below.

Supplementary Figure S10

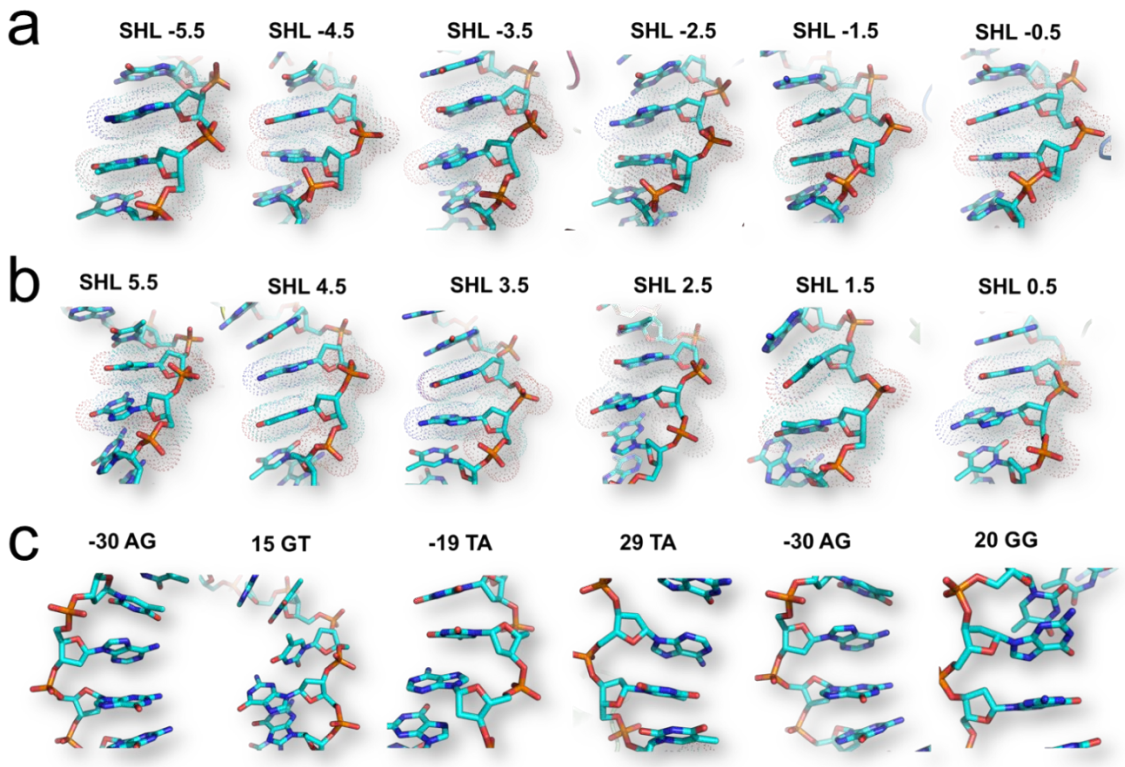

Supplementary Figure S10. Base step deviations in Telo-NCP. The DNA is shown as sticks and the base steps at the pressure points in the minor groove are highlighted with dots. (**a**) The base steps at pressure points in the positive half of the NCP SHL 0 to 5.5. (**b**) The base steps at pressure points in the negative half of the NCP SHL 0 to −5.5. (**c**) Examples of structures of base-pair steps that show highly pronounced deviation from the parameters of an ideal B-form DNA.

Supplementary Figure S11

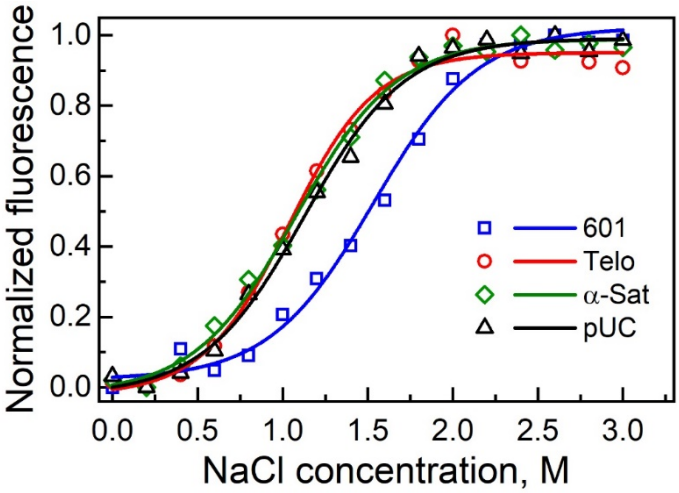

Supplementary Figure S11. Salt-dependent stability of different NCPs in NaCl buffer (20 mM Tris (pH 7.5), 1 mM EDTA, 1 mM DTT, NaCl was varied from 0 to 3 M) measured by tyrosine fluorescence at 305 nm. The 601-NCP is shown in blue, Telo-NCP in red, Telo-NCP bound with cisplatin in yellow, α-sat-NCP in green and pUC-NCP in black. Each curve represents an average of three runs. Five measurements were obtained for each data point in individual runs. In reconstitutions of all NCPs, the same batch of histone octamer was used.

Supplementary Figure S12

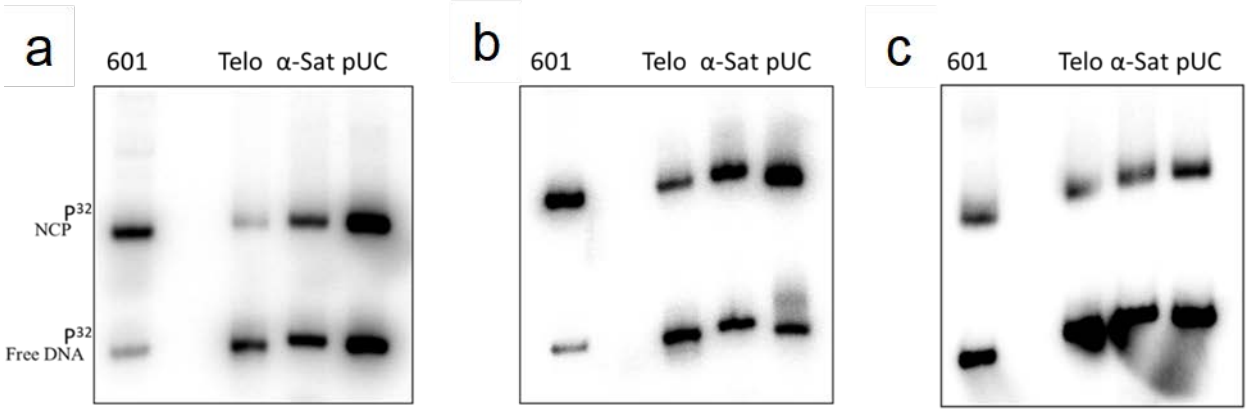

Supplementary Figure S12. Competitive NCP reconstitution. In all gel images, lanes marked 601, Telo, α-sat and pUC show respective reconstituted NCPs and radiolabelled DNA not included in the NCP. **(a)** The PAGE analysis of competitive reconstitution in LiCl using radiolabelled DNA. In salt dialysis, most of the labelled 601 DNA is reconstituted into NCP. In comparison with 601 DNA, pUC and α-sat lanes show a higher ratio of free DNA to NCP indicating that a lower proportion of DNA was incorporated into the NCP. The ratio of free DNA to NCP is lowest for telo DNA suggesting that the least amount of telomeric DNA incorporated into NCP. **(b)** The PAGE analysis of competitive reconstitution in LiCl supplemented with 1 mM $MgCl_2$ using radiolabelled DNA. With the addition of $Mg^{2+,}$ there is a minor increase in the amount of DNA incorporated into NCP for all four DNA sequences. **(c)** The PAGE analysis of competitive reconstitution carried out using radiolabelled DNA employing Nap1 and ACF after 4 hours incubation. In contrast to salt dialysis, only a small fraction of the DNA is incorporated into nucleosome for all four DNA.

Supplementary Figure S13

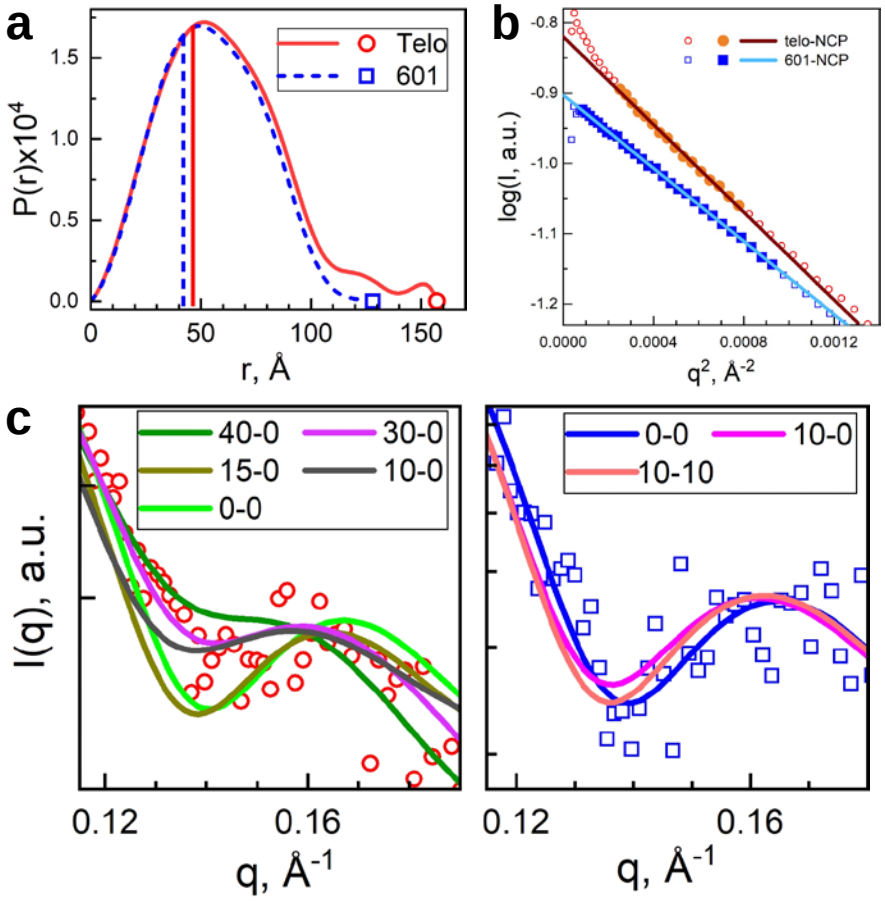

Supplementary Figure S13. Solution SAXS studies of Telo-NCP and 601-NCP. **(a)**. Comparison of the distance distribution functions, P(r), calculated from the solution SAXS profiles of Telo-NCP (1 mg/mL, red symbol and lines) 601-NCP (1 mg/mL, blue symbol and dashed lines). Vertical lines indicate the values of the corresponding R_g. The points indicate the values of D_{max} (maximal pair distance) of each NCP type. Numerical values are given in Supplementary Table S4. (**b**). Example of Guinier plots calculated from the SAXS spectra of the Telo-NCP and 601-NCP solutions shown in Fig. 7 of the main text. Points used for linear fitting are displayed as solid symbols; calculated Rg values are given in Supplementary Table S4. (**c**). Comparison of SAXS profiles recorded at 1 mg/mL NCP concentration at low salt (10 mM KCl) for the Telo-NCP (left panel) and 601-NCP (right panel). Experimental data are shown as points and form factors calculated from molecular structures as curves. For the modelled curves, two numbers show the lengths of DNA base pairs unwrapped form the entry/exit of the NCP. For the Telo-NCP the form factors of the NCPs with asymmetric DNA positioning or unwinding of up to 40 bp give the best fitting to the experimental data. For the 601-NCP, the best fit is observed with the NCP structures showing no or small distortion from the fully wrapped DNA conformation. Numerical data is given in Supplementary Table S4.

Supplementary Table S4. Comparison of the outputs from SAXS profiles obtained for the Telo-NCP and 601-NCP in experiment and simulated from modelled molecular structures, including the radius of gyration *(R_g)* and the maximal intra-atom distances within a particle (*D_{max}*) determined from the distance distribution function *P(r)*. The top row of numbers shows parameters obtained from the experiment; two sections below present output of the analysis of molecular structures constructed from stretches of straight DNA and NCP structure generated from crystal structures or from MD simulations. Best fittings of the modelled form factors to the experimental SAXS profiles are highlighted by bold font.

Number of unwrapped bp	R_g from Guinier plot, Å	R_g from P(r), Å	D_{max}, Å	χ^2, fit quality,
Data extracted from SAXS measurement 601-NCP, 1.0 mg/mL				
Experiment	**42.1** +/– 0.1	**42.1** +/– 0.1	**128**	0.986, excellent
NCP crystal structures				
3LZ0	39.8	39.9	117	8.15
Telo-NCP	39.7	38.8	116	8.56
NCP structures with collapsed tails generated in MD simulations				
0-0	41.6	40.8	117	**1.05**
10-0	42.5	42.1	132	**1.69**
10-10	42.4	42.0	132	**1.74**
15-0	42.9	42.5	131	2.09
20-0	44.0	43.6	138	2.87
15-15	44.1	43.7	143	3.50
Data extracted from SAXS measurement Telo-NCP, 1.0 mg/mL				
Experiment	**46.3** +/– 0.2	**46.4** +/– 0.2	**157**	0.840, good
NCP crystal structures				
3LZ0	39.8	39.9	117	15.26
Telo-NCP	39.7	38.8	116	16.72
NCP structure with collapsed tails generated in MD simulations				
40-0	50.4	50.3	199	**1.44**
30-0	46.1	45.8	166	**1.66**
0-0	41,1	40.8	130	2.57
10-0	41.9	41.6	132	2.66
15-0	42.0	41.8	131	2.66
25-0	44.4	44.1	154	2.65
10-10	42.1	41.8	132	3.20
15-15	43.4	43.1	143	3.81
20-20	43.6	43.4	140	4.36

SUPPLEMENTARY REFERENCES

1. Ong, M.S., Richmond, T.J. and Davey, C.A. (2007) DNA stretching and extreme kinking in the nucleosome core. *J. Mol. Biol.*, **368**, 1067-1074.
2. Vasudevan, D., Chua, E.Y. and Davey, C.A. (2010) Crystal structures of nucleosome core particles containing the '601' strong positioning sequence. *J. Mol. Biol.*, **403**, 1-10.
3. Chua, E.Y., Vasudevan, D., Davey, G.E., Wu, B. and Davey, C.A. (2012) The mechanics behind DNA sequence-dependent properties of the nucleosome. *Nucleic Acids Res.*, **40**, 6338-6352.
4. Olson, W.K., Gorin, A.A., Lu, X.J., Hock, L.M. and Zhurkin, V.B. (1998) DNA sequence-dependent deformability deduced from protein–DNA crystal complexes. *Proc. Natl. Acad. Sci. U.S.A.*, **95**, 11163-11168.